Supplemental Material for:

Formation of a Reactive, Alkyl Thiolate-Ligated Fe^{III}-Superoxo Intermediate Derived from Dioxygen

Maike N. Blakely, Maksym A. Dedushko, Penny Chaau Yan Poon, Gloria Villar-Acevedo, and Julie A. Kovacs*

Experimental Details

General Methods. All reactions were performed under an atmosphere of dinitrogen in a glove box, or using a custom–built two-neck solution sample holder equipped with a threaded glass connector (sized to fit an ATR probe). Reagents purchased from commercial vendors were of the highest purity available, and used without further purification. Methylene chloride (DCM), tetrahydrofuran (THF), diethyl ether (Et_2O), and acetonitrile (MeCN) were rigorously degassed, and purified using solvent purification columns housed in a custom stainless-steel cabinet, dispensed via a stainless steel schlenk-line (GlassContour). 2-Methyltetrahydrofuran (Me-THF) was distilled under an inert atmosphere from Na/benzophenone and degassed with argon prior to use. Methanol (MeOH) was distilled from magnesium methoxide and degassed prior to use. ^{1}H NMR spectra were recorded on a Bruker AV 300 FT-NMR spectrometer and are referenced to an external standard of TMS (paramagnetic compounds). Chemical shifts are reported in ppm and coupling constants (J) in Hz. EPR spectra were recorded on a Bruker EPX CW-EPR spectrometer operating at X-band frequency at 120 K. The EPR spectra were simulated using EasySpin (version 5.2.23), a computational package developed by Stoll and Schweiger[1] and based on Matlab (The MathWorks, Massachusetts, USA). Cyclic voltammograms were recorded in MeCN (100 mM $NBu_4(PF_6)$ solutions) on a PAR 273 potentiostat utilizing a glassy carbon working electrode, platinum auxiliary electrode, and an SCE reference electrode. Magnetic moments (solution state) were obtained using the Evans' method as modified for super-conducting solenoids.[2,3] Electronic absorption spectra were recorded using a Varian Cary 50 spectrophotometer equipped with a fiber optic cable connected to a C-technologies ATR probe.

Synthesis of $[Fe^{II}(S_2^{Me2}N_3(Pr,Pr)]$ (2) 3-methyl-3-mercapto-2-butanone (0.38 g, 3.2 mmol) was dissolved in 10 ml of MeOH. To this NaOMe (0.172 g, 3.2 mmol) was added and the mixture was stirred for 10 min then 3,3'-iminobis (propylamine) (0.21 ml, 1.5 mmol) was added. After stirred for 20 mins at room temperature, this solution of organics was cooled to -40 ^oC for over 1 hour. This solution was added dropwise to a solution of anhydrous ferrous chloride (0.19 g, 1.5 mmol) in 10 ml of MeOH also cooled to -40^oC for over 1 hour. The combined solutions were allowed to stir for 3 hours at room temperature before being stored in the freezer overnight. The solution was filtered through a bed of Celite, the solvent was removed by vacuum. The resulting crude black powder was dissolved in a minimal amount of cooled MeCN and the undissolved

salts were then removed by filtering through a bed of Celite. The solvent was removed by vacuum then <4 mL of THF was added and layered with 15 mL of pentane and cooled at -40°C for ~12 h to afford 0.438 g (1.13 mmol, 76 %) of green-brown micro-crystalline solid. Electronic absorption (THF): λ_{max} (ε, M^{-1} cm^{-1}) = 420 nm (1509). IR υ(cm^{-1}): 1636 (imine). Cyclic Voltammetry: $E_{1/2}$ (MeCN) = -425 mV vs SCE. Solution magnetic moment (298 K; MeCN): μ_{eff} = 2.63 μ_B.

Formation of [$Fe^{III}(S_2^{Me2}N_3$(Pr,Pr)-O_2] (4) via the addition of O_2 to 1. A 0.238-0.476 mM solution of **2** was prepared in THF or DCM under an inert atmosphere in a drybox. The resulting solution was transferred via gastight syringe to a custom-made two-neck vial equipped with a septum cap and threaded dip-probe feed-through adaptor that had been previously been purged with argon. This solution was cooled in an acetone and dry ice bath to -73 ˚C. Argon stream was removed then to the vial 5 mL of pure O_2 was bubbled through the solution over the course of 30 seconds, resulting in the formation of metastable **4**.

Formation of [$Fe^{III}(S_2^{Me2}N_3$(Pr,Pr)-O_2] (4) via the addition of KO_2 to 2. A 0.238-0.476 mM solution of **2** was prepared in THF under an inert atmosphere in a drybox. The resulting solution was transferred via gastight syringe to a custom-made two-neck vial equipped with a septum cap and threaded dip-probe feed-through adaptor that had been previously been purged with argon. This solution was cooled in an acetone and dry ice bath to -73 ˚C. A slurry of 1.1-50 eq. KO_2 in the presence of 18-crown-6 in 100 µL of THF was added via a gas tight syringe resulting in the formation of metastable **4**.

Azide Inhibition Studies. A 0.476 mM solution of **1** was prepared in THF under an inert atmosphere in a drybox. The resulting solution was transferred via gastight syringe to a custom-made two-neck vial equipped with a septum cap and threaded dip-probe feed-through adaptor that had been previously been purged with argon. This solution was cooled in an acetone and dry ice bath to -73 ˚C. A solution containing 50 eq. NaN_3 in 100 µL of THF was added via a gas tight syringe. Argon stream was removed then to the vial 5 mL of pure O_2 was bubbled through the solution over the course of 30 seconds, resulting in the formation of previously reported [$Fe^{III}(S_2^{Me2}N_3$(Pr,Pr)-N_3],[4] as opposed to superoxo **4**.

Hydrogen Atom Transfer (HAT) Reactions. Aliquots of **1** in THF or d^8-THF (1 mL of a 0.476 mM solution) were used to generate **4** from O_2 as stated above. Kinetic measurements were

started immediately after generation of **4**. Reactions between **4** and H-atom donors were monitored by electronic absorption spectroscopy, and involved pseudo first-order conditions (with respect to Fe) at -73 ˚C, with the H-atom donors held in excess (CHD: 47.6 mM; THF: 12.3 M). Pseudo first-order plots monitored the decrease in absorbance at λ= 523 nm.

Resonance Raman Experiments. Resonance Raman (rR) spectra were obtained from the frozen solution samples at liquid nitrogen temperature (77 K) in a backscattering sample geometry. The visible excitation wavelength at 527 nm is provided by the CW (continuous wave) output of the second harmonic of neodymium-doped yttrium lithium fluoride (Nd:YLF) laser (Photonics Industries International, GM-30–527). Laser power at the sample varies from 1.4 to 6.0 mW. The scattered light from the sample was collected and focused onto a triple spectrograph (Spex 1877) equipped with a CCD detector (Roper Scientific, Model 7375-0001) operating at -110° C. Spectra were calibrated with dimethylformamide and acetone. The laser line of 527 nm was chosen to be in the proximity of the absorption spectrum of the transient intermediates probed. Sample concentrations were 5-10 mM were added to the quartz EPR sample tubes. The samples were cooled to 77 K in a quartz liquid nitrogen finger dewar and hand spun to minimize sample decomposition during scan collection. Resonance Raman spectra were processed with Spectragryph software.

Spin Quantitation of EPR Spectra. The X-band EPR spectra were recorded on a Bruker EMX CW-EPR spectrometer equipped with a N_2 gas flow cryostat. Spectra were collected at 120 K using the following parameters: 9.28 GHz frequency, 2.0 mW power, 6×10^4 gain, 100 kHz modulation frequency, 0.2 mT modulation amplitude, and 40.96 ms conversion time. The EPR spectra were simulated using EasySpin (version 5.2.23), a computational package developed by Stoll and Schweiger.[1] Double integration of EPR signals were carried out using Matlab (The MathWorks, Massachusetts, USA).

Samples of **3** for quantification of spin concentration were prepared as follows. A 1.0 mM solution of **1** was prepared in 98:2 THF:Me-THF under an inert atmosphere in a drybox. 0.5 mL of the resulting solution was then transferred into EPR tubes, and 2 mL of pure O_2 was bubbled through the solution at 293 K over the course of 30 seconds, and left to react for 10 mins, resulting in the formation of **3**.

Samples of **5** for quantification of spin concentration were prepared as follows. A 1.0 mM solution of **1** was prepared in 98:2 THF:Me-THF under an inert atmosphere in a drybox. 0.5 mL of the resulting solution was transferred into EPR tubes. This solution was cooled to -73 ˚C in an

acetone/dry ice bath, and 2 mL of pure O_2 was then bubbled through the solution over the course of 30 seconds, and left to react for 40 mins, resulting in the formation of metastable **5**.

Quantification of the unpaired spin concentration within a sample was achieved by comparison of the double integral of the EPR intensity to that of a standard curve made from solutions of 0.25 mM-1.4mM azide-bound[4] $[Fe^{III}(S_2{}^{Me2}N_3(Pr,Pr)(N_3)]$ in 98:2 THF:Me-THF.

X-ray Crystallographic Structure Determination. A yellow green prism, measuring 0.32 x 0.03 x 0.03 mm^3 was mounted on a loop with oil. Data was collected at -173°C on a Bruker APEX II single crystal X-ray diffractometer, Mo-radiation. Crystal-to-detector distance was 40 mm and exposure time was 180 seconds per frame for all sets. The scan width was 1°. Data collection was 100% complete to 25° in ϑ. A total of 32, 245 reflections were collected covering the indices, -23<=h<=23, -11<=k<=11, -25<=l<=25. 3547 reflections were symmetry independent and the elevated R_{int} = 0.04355 indicated that the data was of better than average quality (0.07). Indexing and unit cell refinement indicated a primitive orthorhombic lattice. The space group was found to be Pbca (No. 61).

The data was integrated and scaled using SAINT, SADABS within the APEX2 software package by Bruker.[5] Solution by direct methods (SHELXS, SIR97) produced a complete heavy atom phasing model consistent with the proposed structure.[6,7] The structure was completed by difference Fourier synthesis with SHELXL.[8,9] Scattering factors are from Waasmair and Kirfel.[10] Hydrogen atoms were placed in geometrically idealized positions and constrained to ride on their parent atoms with C---H distances in the range 0.95-1.00 Angstrom. Isotropic thermal parameters U_{eq} were fixed such that they were $1.2U_{eq}$ of their parent atom Ueq for CH's and $1.5U_{eq}$ of their parent atom U_{eq} in case of methyl groups. All non-hydrogen atoms were refined anisotropically by full-matrix least-squares. Final solution plotted using ORTEP and POV-Ray programs.

Computational Details. Calculations were performed using the ORCA v. 4.0.0 quantum chemistry package developed by Neese and coworkers,[11] and employed a polarized triple-zeta def2-TZVP basis set, the def2/J auxiliary basis set for Coulomb fitting, and the atom-pairwise dispersion correction of Grimme (D3BJ).[12] Tight convergence criteria were required for self-consistent field (SCF) solutions. The Grid4 (GridX4) integration grid size, and the conductor-like polarizable continuum model with the dielectric constant ε = 7.25 for tetrahydrofuran solvent (CPCM(THF)), were used for geometry optimizations.[13] Geometry optimizations and analytical frequency calculations were performed using the PBE0 functional, with the resolution of identity (RI) chain-of-spheres (RIJCOSX) approximation,[14,15] and initiated from the crystallographic

coordinates when available. Analytical frequency calculations were performed on all optimized structures to determine whether the obtained stationary points corresponded to local minima.

Previously reported[4] crystallographically determined structure of azide-bound $[Fe^{III}(S_2{}^{Me2}N_3(Pr,Pr))(N_3)]$ was used as a starting point for the calculated superoxo-bound structure, $[Fe^{III}(S_2{}^{Me2}N_3(Pr,Pr))(O_2)]$. Specifically, the distal azide nitrogen N(6) atom was deleted, and the proximal N(4) and middle N(5) atoms were replaced with oxygen atoms. The Fe(III) metal center was assumed to be in the S = ½ state. A low spin-state was shown previously to be stabilized with thiolate-ligated Fe(III) complexes due to the thiolate's nephelauxetic effect.[4,16-18] Based on optimized bond lengths reported for arylthiolate-ligated $[Fe^{III}(LN_3S(O_2))]$,[19] $r_{Fe\text{-}O}$ and $r_{O\text{-}O}$ were set to 2.089 Å, and 1.290 Å, respectively, as a starting point.

Calculations for the Fe(III)-superoxo complex, $[Fe^{III}(S_2{}^{Me2}N_3(Pr,Pr)(O_2)]^+$ (**4**) employed the broken-symmetry formalism to model coupled paramagnetic sites. An SCF calculation was first performed for the high spin (HS) state of the iron-superoxo complex, $Fe^{III}(S$ = ½, ↑)-$O_2{}^{\bullet-}$ (S = ½, ↑). Next, a broken symmetry state was set up with the spin-flip chosen at the iron center (final total m_s = 0) and another SCF calculation was ran to calculate energy of the "broken symmetry" (BS), $Fe^{III}(S$ = ½, ↓)-$O_2{}^{\bullet-}$ (S = ½, ↑), state. Finally, the energies of both HS and BS states were used to estimate the coupling constant, J, (associated with the phenomenological Hamiltonian $\hat{H} = -2J_{12}\hat{S}_1\hat{S}_2$) using the equation $J = -(E_{HS} - E_{BS})/(\langle S^2\rangle_{HS} - \langle S^2\rangle_{BS})$, which is valid over the entire coupling strength regime. E_{HS} and E_{BS} are the energies of the high-spin (HS), and the broken-symmetry (BS) states, respectively, and $\langle S^2\rangle$ are the expectation values of the squared spin operator for the HS and BS states.[20] The coupling constant of J^{calc} = – 450 cm^{-1} was obtained for putative **4**, consistent with its ⊥-mode EPR silence at 117 K.

Hybrid time-dependent DFT (TD-DFT) calculations employed the RIJCOSX and the Tamm-Dancoff approximations (TDA).[21,22] The Fermi level, i.e., the halfway between the calculated HOMO and LUMO energies, was set to 0 eV in molecular orbital (MO) analysis. Excited states from TD-DFT calculations were analyzed using Natural Transition orbitals (NTOs) and by visualizing their difference densities between the ground and excited states. Canonical molecular orbital isosurfaces and natural transition orbitals in the TD-DFT calculations were visualized at an isovalue of 0.05 $a_0{}^3$ using UCSF Chimera.[23]

Gaussian v.16 was used to calculate resonance Raman frequencies, and isotope displacements for $[Fe^{III}(S_2{}^{Me2}N_3(Pr,Pr)(O_2)]^+$. A UPBE1PBE functional, and a polarized triple-

zeta def2-TZVP basis set were employed to calculate analytical vibrational frequencies (freq = (raman, anharmonic)). Analytical frequencies of the isotopically substituted $[Fe^{III}(S_2{}^{Me2}N_3(Pr,Pr)(^{18}O_2)]^+$ complex were performed by specifying the mass (iso = 17.999) of the oxygen atoms in the geometry input file.

Supplemental Figures

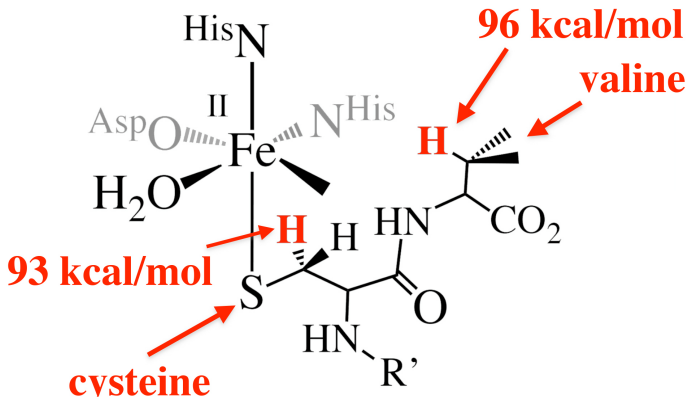

Figure S1. Active site of the substrate-bound form of IPNS, showing the C-H bonds cleaved by dioxyen intermediates and their dissociation energies (BDE), as well as the vacant coordination site *trans* to the aspartate oxygen and *cis* to the cysteinate sulfur.

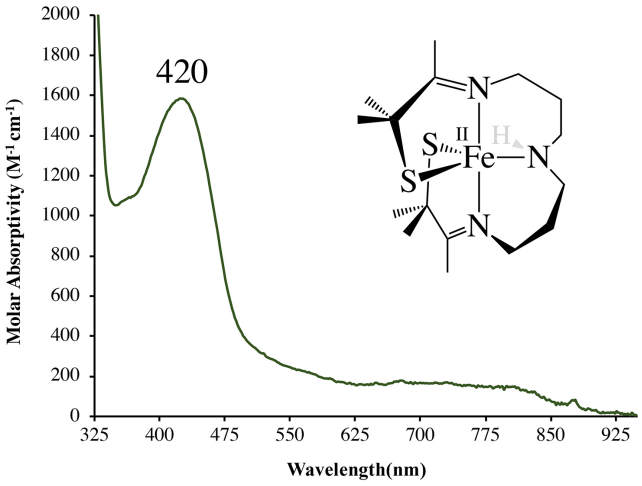

Figure S2. Qunatitative electronic absorption spectra of 0.238 mM $[Fe^{II}(S_2{}^{Me2}N_3(Pr,Pr)]$ (**1**) in THF at 200 K.

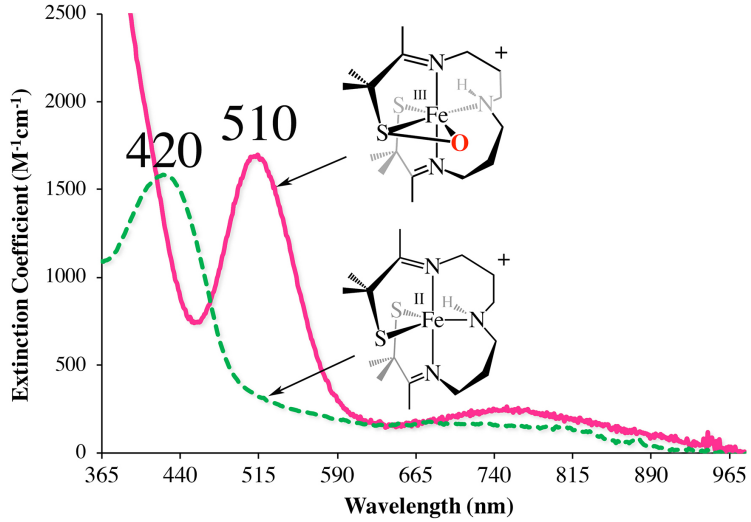

Figure S3. Quantitative electronic absorption spectrum of 0.238 mM of [$Fe^{II}(S_2{}^{Me2}N_3(Pr,Pr)$] (**1**) vs [$Fe^{III}$ (η^2-$S^{Me2}O$)(S^{Me2})N_3(Pr,Pr)]$^+$ (**3**) in THF at 295 K.

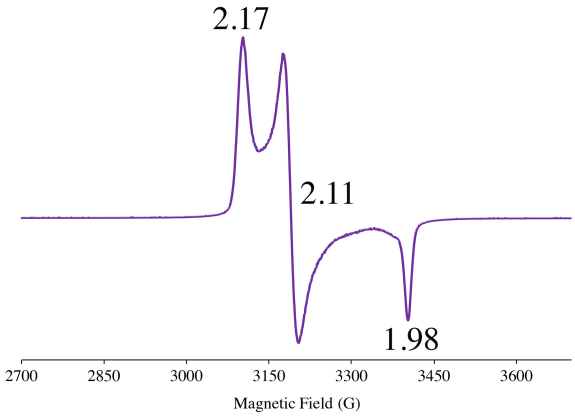

Figure S4. EPR (98:2 THF:Me-THF, 117 K, X-Band) spectrum of the product formed in the reaction between 1.0 mM reduced [$Fe^{II}(S_2{}^{Me2}N_3(Pr,Pr)$] (**1**) and dioxygen ($O_2$) in 98:2 THF:Me-THF at 298 K..

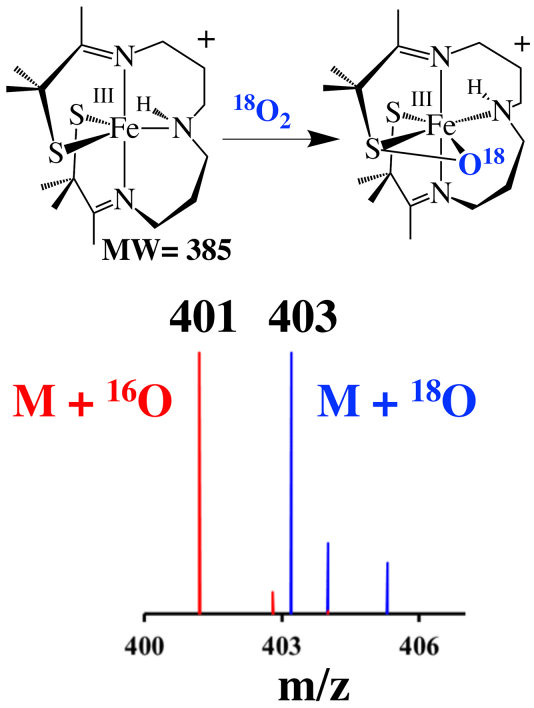

Figure S5. Positive mode electrospray ionization mass spectrum of [$Fe^{III}(\eta^2$-S^{Me2} $^{18}O)(S^{Me2})N_3(Pr,Pr)]^+$ (blue line) generated from **1** and $^{18}O_2$. The ^{16}O-derivative, [$Fe^{III}(\eta^2$-S^{Me2} $^{16}O)(S^{Me2})N_3(Pr,Pr)]^+$ (red line), forms via exchange of the sulfenate oxygen with $H_2{}^{16}O$ on the mass spec instrument column. Sulfenic acids, RS-OH, are known to be labile (BDE(S-O) = 74.9 kcal/mol)[24] and prone to nucleophilic displacement by OH^-.[25,26]

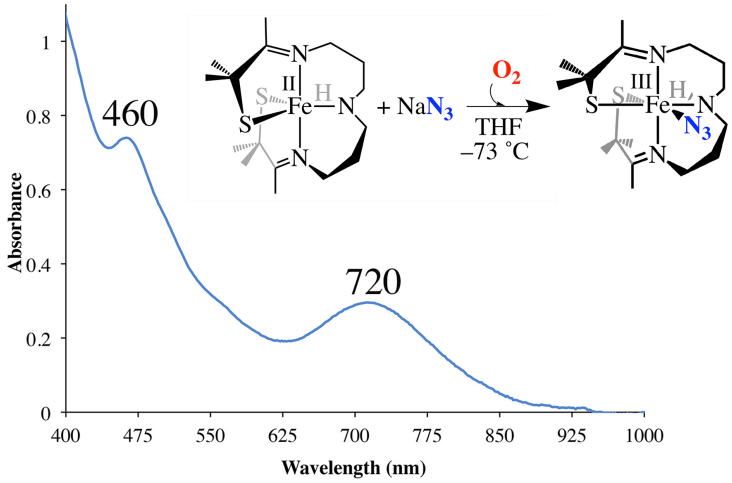

Figure S6. Azide inhibits the formation of **3** in the reaction between reduced [$Fe^{II}(S_2{}^{Me2}N_3(Pr,Pr)$] (**1**) and instead results in outer sphere oxidation of the metal to form previously reported azide-bound [$Fe^{III}(S_2{}^{Me2}N_3(Pr,Pr)(N_3)]^+$.[4]

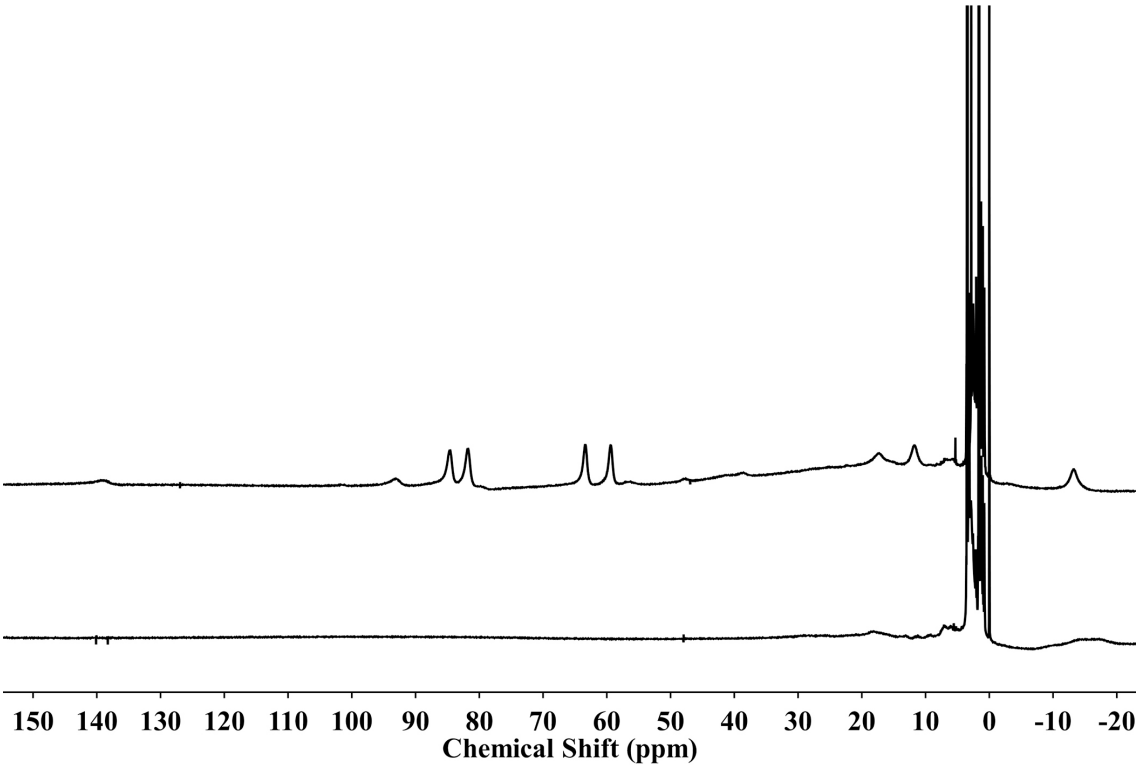

Figure S7. The paramagnetically shifted signals in the ^{1}H NMR (500 MHz) of **1** (top) collapse to diamagnetic signals upon the addition of O_2 and formation of intermediate **4** (bottom) in d^8-THF at -40 ˚C.

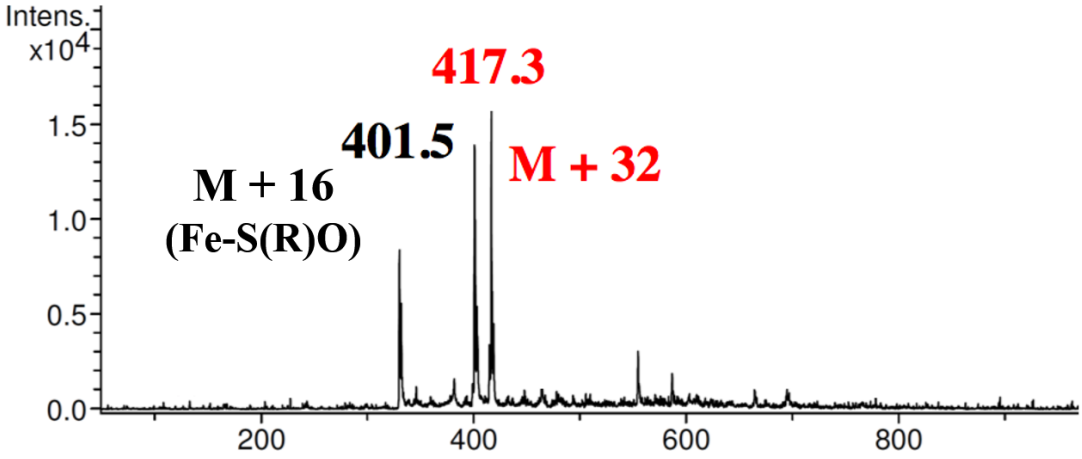

Figure S8. Positive mode ESI-MS spectrum of **4** generated from **1** and $^{16}O_2$. (M refers to the parent ion **1**, which has an m/z = 385). Slight warming during sample injection resulted in its partial conversion to the sulfenate $Fe^{III}S(R)O$ product **3**, as indicated by the M+16 peak.

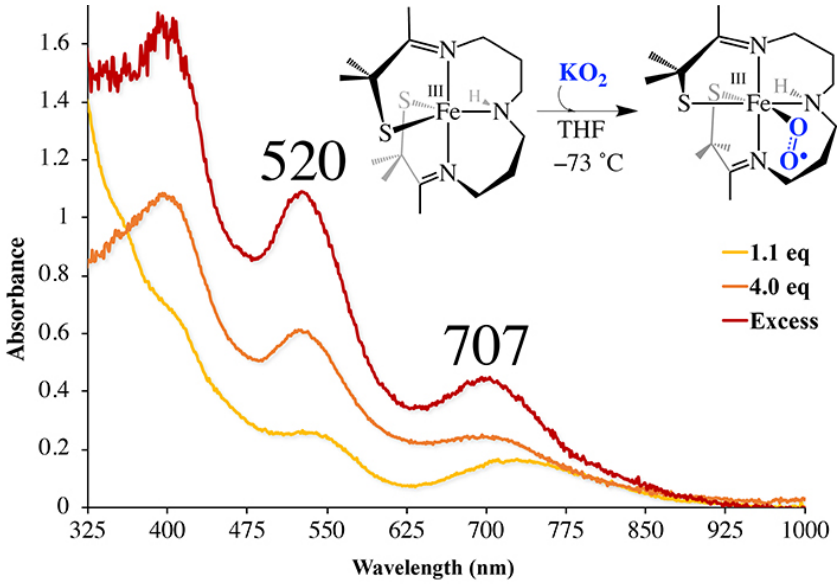

Figure S9. An intermediate forms, which is identical to that formed in the reaction between reduced [$Fe^{II}(S_2{}^{Me2}N_3(Pr,Pr)$] (**1**) and O_2, upon the addition of excess (50 equiv) KO_2 (solubilized in THF with 18-cr-6) to oxidized [$Fe^{III}(S_2{}^{Me2}N_3(Pr,Pr)]^+$ (**2**).

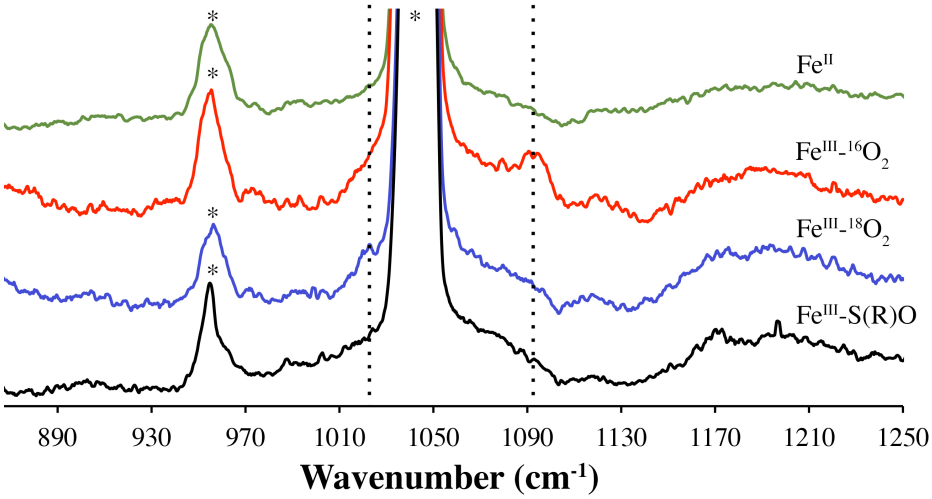

Figure S10. Comparison of the rR spectra of [$Fe^{II}(S_2{}^{Me2}N_3(Pr,Pr)$] (**1**), the metastable intermediate (10 mM) formed with $^{16}O_2$, the metastable intermediate formed with $^{18}O_2$, and the product, [$Fe^{III}(RS^{Me2}O)(S^{Me2})N_3(Pr,Pr)]^+$ (**3**) in CD_2Cl_2 at 77 K, excitation wavelength $\boldsymbol{\lambda}^{ex}$ = 527 nm; 6 mW power. Verticle dotted lines mark the $\boldsymbol{\nu}_{16O\text{-}16O}$ stretch at 1093 cm^{-1}, and the $\boldsymbol{\nu}_{16O\text{-}16O}$ stretch at 1022 cm^{-1}. *= solvent peak. Experimental $\Delta(^{16}O\text{-}^{18}O)$= 71 cm^{-1} versus calculated $\Delta(^{16}O\text{-}^{18}O)$ = 72 cm^{-1} using Hooke's law.

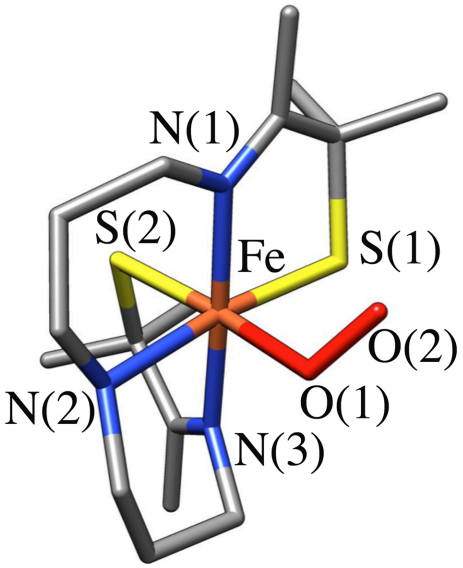

Figure S11. Broken symmetry DFT (BS-DFT) (PBE0/def2-TZVP) optimized structure of putative *S* = 0 superoxo compound $[Fe^{III}(S_2{}^{Me2}N_3(Pr,Pr)(O_2)]^+$ (**4**).

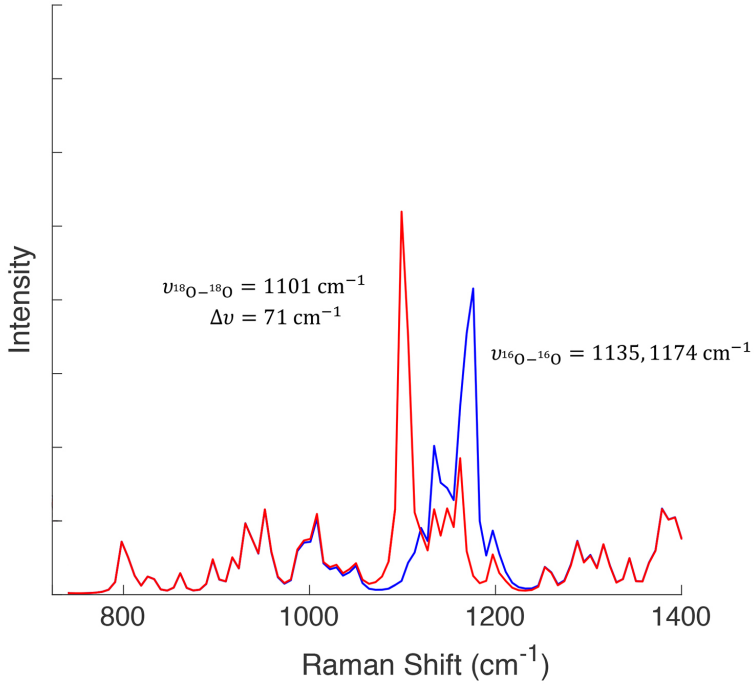

Figure S12. TD-DFT calculated (Gaussian v.16, UPBE1PBE functional, and a polarized triple-zeta def2-TZVP basis set) frequencies, and isotope displacements for $[Fe^{III}(S_2{}^{Me2}N_3(Pr,Pr)(O_2)]^+$ (**4**) and its $^{18}O_2$-derivative.

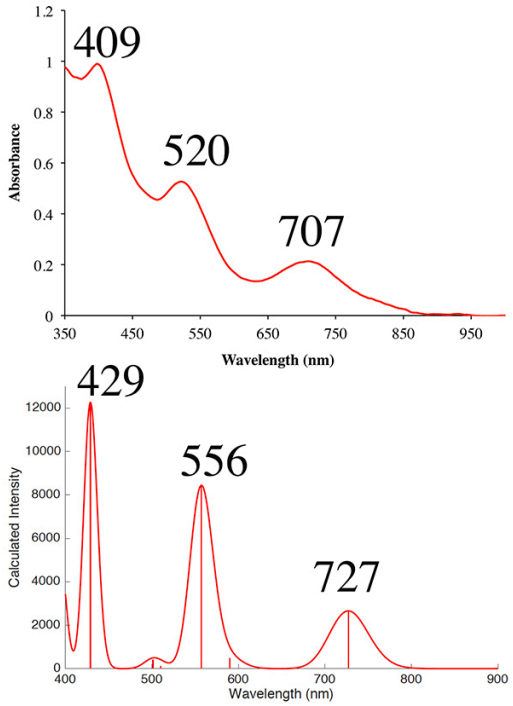

Figure S13. Comparison of the TD-DFT calculated spectrum (bottom) with the experimental spectrum of superoxo complex $[Fe^{III}(S_2{}^{Me2}N_3(Pr,Pr)(O_2)]^+$ (**4**).

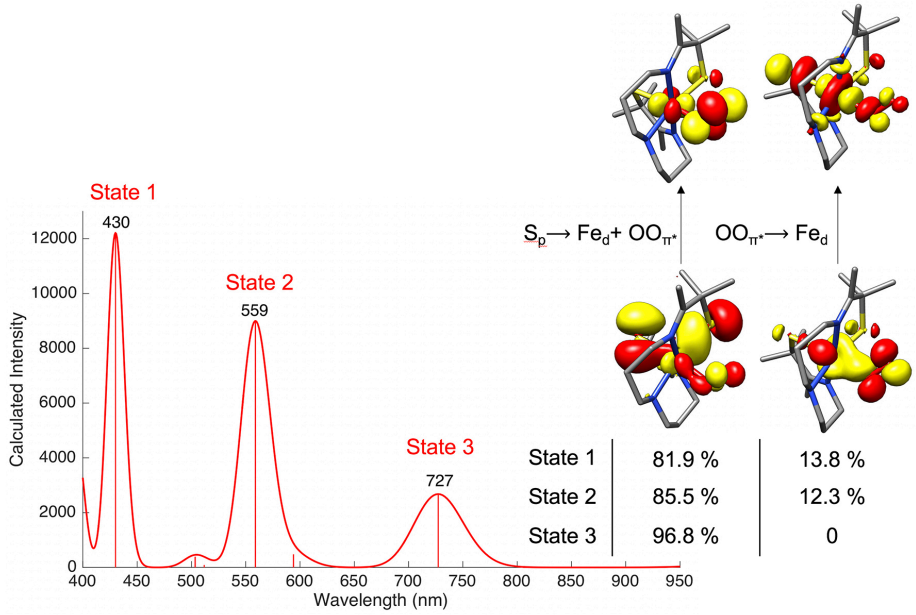

Figure S14. TD-DFT calculated electronic absorption spectrum of superoxo complex $[Fe^{III}(S_2{}^{Me2}N_3(Pr,Pr)(O_2)]^+$ (**4**) including natural transition orbitals (NTO) describing the charge transfer (CT) transitions, showing that States 1 and 2 have both π^*(O-O)→ d_{xy}(Fe), and RS^- →Fe-$O_2^{\bullet-}$ charge transfer character, whereas the lower energy transition, State 3, is only RS^- →Fe-$O_2^{\bullet-}$ charge transfer in character.

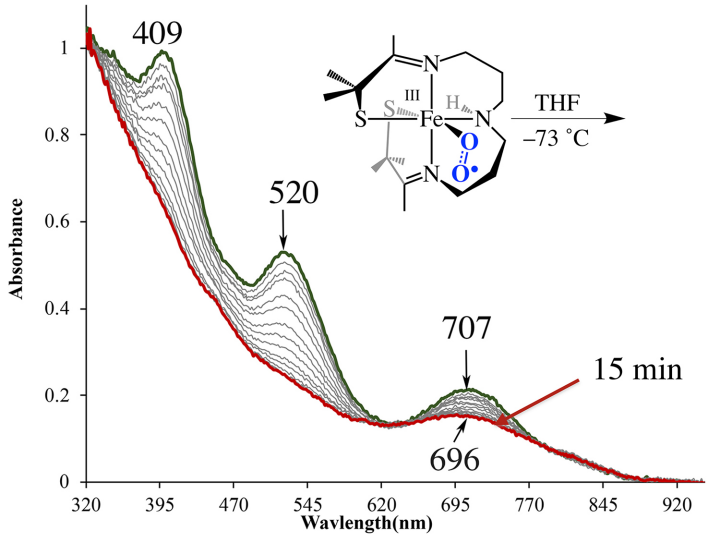

Figure S15. Conversion of $[Fe^{III}(S_2{}^{Me2}N_3(Pr,Pr)(O_2)]^+$ (**4**) to a second metastable intermediate, **5**, at -73 ˚C in THF.

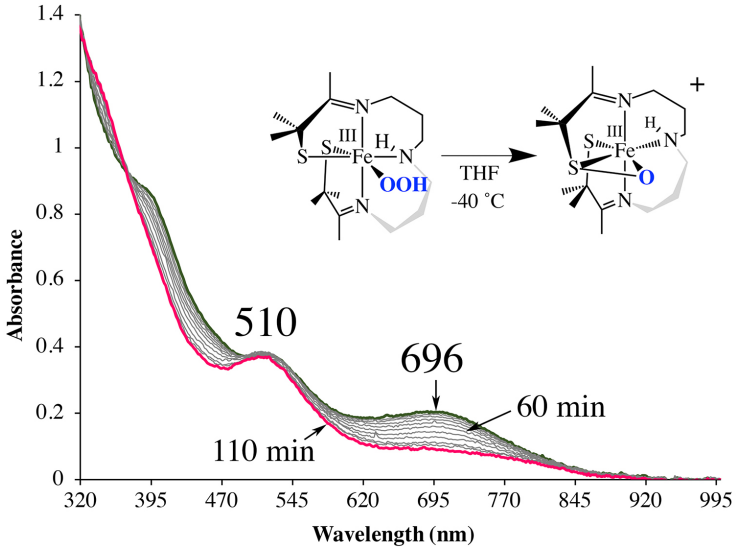

Figure S16. Conversion of putative hydroperoxo $[Fe^{III}(S_2{}^{Me2}N_3(Pr,Pr)(OOH)]^+$ (**5**) to the final sulfenate product **3** in THF requires warming to -40 ˚C in order for the reaction to take place at reasonable rates.

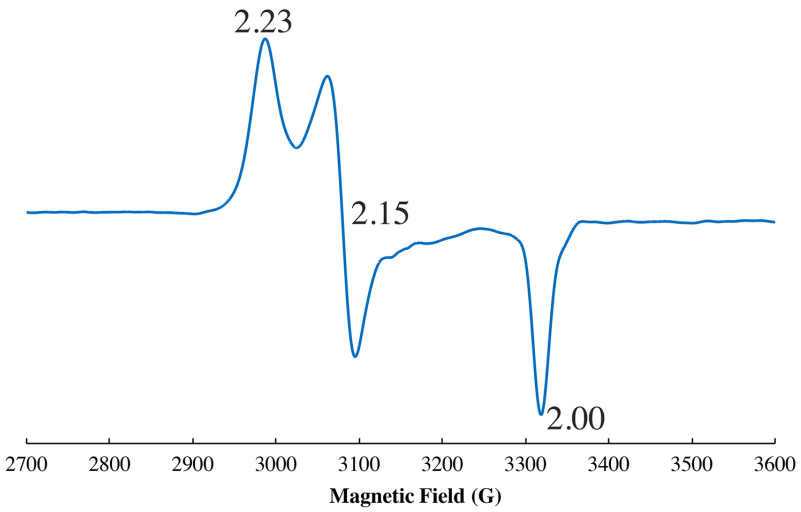

Figure S17. X-band EPR spectrum (⊥-mode) of putative hydroperoxo Fe(III)-OOH (**5**), formed via the abstraction of a H-atom by superoxo Fe(III)-$O_2^{\bullet}$ (**4**). Spin quantitation, using double integration and a calibration curve (Figure S18) indicates that this signal corresponds to 87% of the sample.

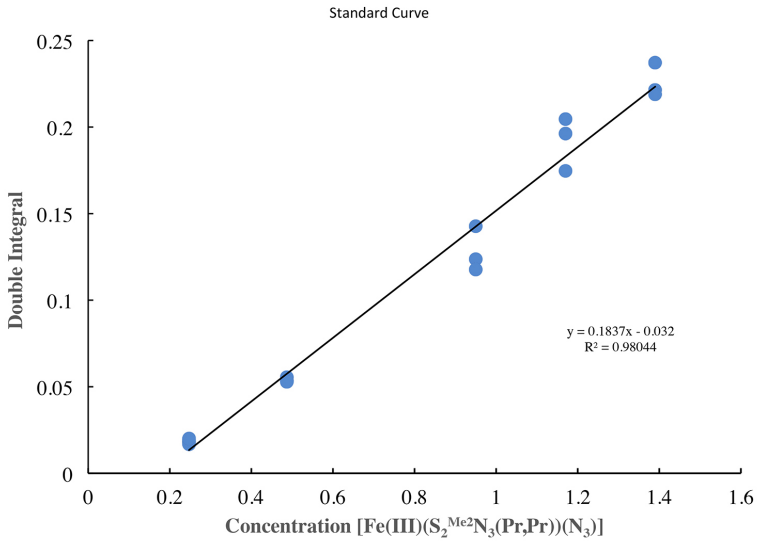

Figure S18. Calibration curve for the double-integral of the S= ½ EPR signal of azide-bound $[Fe^{III}(S_2^{Me2}N_3(Pr,Pr))(N_3)]$ versus concentration.

Supplemental Tables

Table S1. DFT Optimized Bond Lengths for [$Fe^{III}(S_2^{Me2}N_3(Pr,Pr)(O_2)$] (**4**).

	Calculated Bond Length (Å)
Fe-S(1)	2.203
Fe-S(2)	2.256
Fe-O(1)	1.947
O(1)-O(2)	1.289
Fe-N(1)	1.981
Fe-N(2)	2.111
Fe-N(3)	1.973

Table S2. Crystal Data for [$Fe^{II}(S_2{}^{Me2}N_3(Pr,Pr)$] (**1**).

Empirical formula	C16 H31 Fe N3 S2	
Formula weight	385.41	
Temperature	100(2) K	
Wavelength	0.71073 Å	
Crystal system	Orthorhombic	
Space group	Pbca	
Unit cell dimensions	a = 19.5588(9) Å	α= 90°
	b = 9.3044(5) Å	β= 90°
	c = 21.1744(10) Å	γ = 90°
Volume	385.4(3) $Å^3$	
Z	8	
Density (calculated)	1.329 Mg/m^3	
Absorption coefficient	1.000 mm^{-1}	
F(000)	1648	
Crystal size	0.26 x 0.20 x 0.20 mm^3	
Theta range for data collection	1.924 to 25.400°.	
Index ranges	-23<=h<=23, -11<=k<=11, -25<=l<=25	
Reflections collected	32245	
Independent reflections	3547 [R(int) = 0.0435]	
Completeness to theta = 25.00°	100.0 %	
Max. and min. transmission	0.646 and 0.745	
Refinement method	Full-matrix least-squares on F^2	
Data / restraints / parameters	3547 / 0 / 209	
Goodness-of-fit on F^2	1.021	
Final R indices [I>2sigma(I)]	R1 = 0.0251, wR2 = 0.0551	
R indices (all data)	R1 = 0.0373, wR2 = 0.0594	
Largest diff. peak and hole	0.371 and -0.288 $e.Å^{-3}$	

Table S3. Atomic coordinates (x 10^4) and equivalent isotropic displacement parameters (A^2 x 10^3) for [$Fe^{II}(S_2{}^{Me2}N_3$(Pr,Pr)] (**1**). U(eq) is defined as one third of the trace of the orthogonalized Uij tensor.

	x	y	z	U(eq)
Fe(1)	1256(1)	4840(1)	1480(1)	12(1)
S(1)	266(1)	6067(1)	1188(1)	17(1)
S(2)	2212(1)	5835(1)	1966(1)	17(1)
N(1)	983(1)	4434(2)	2451(1)	16(1)
N(2)	1399(1)	2534(2)	1445(1)	15(1)
N(3)	1454(1)	5016(2)	469(1)	13(1)
C(6)	425(1)	3394(2)	2536(1)	23(1)
C(7)	665(1)	1891(2)	2375(1)	25(1)
C(8)	833(1)	1623(2)	1690(1)	20(1)
C(9)	1655(1)	1967(2)	836(1)	16(1)
C(10)	2220(1)	2918(2)	572(1)	17(1)
C(11)	1966(1)	4113(2)	148(1)	17(1)
C(12)	1133(1)	5964(2)	147(1)	15(1)
C(14)	596(1)	6909(2)	465(1)	16(1)
C(16)	936(1)	8340(2)	636(1)	23(1)
C(15)	-7(1)	7213(2)	22(1)	21(1)
C(13)	1265(1)	6228(2)	-542(1)	22(1)
C(4)	1293(1)	5050(2)	2904(1)	18(1)
C(1)	1823(1)	6203(2)	2742(1)	17(1)
C(2)	1 441(1)	7643(2)	2708(1)	22(1)
C(3)	2400(1)	6310(3)	3231(1)	27(1)
C(5)	1138(1)	4771(3)	3593(1)	34(1)

Table S4. Bond lengths [A] and angles [deg] for [$Fe^{II}(S_2{}^{Me2}N_3(Pr,Pr)$] (**1**).

Fe(1)-N(1)	2.1556(16)
Fe(1)-N(2)	2.1656(16)
Fe(1)-N(3)	2.1815(15)
Fe(1)-S(2)	2.3263(5)
Fe(1)-S(1)	2.3306(5)
S(1)-C(14)	1.8371(19)
S(2)-C(1)	1.8422(19)
N(1)-C(4)	1.273(2)
N(1)-C(6)	1.470(2)
N(2)-C(9)	1.479(2)
N(2)-C(8)	1.488(2)
N(2)-H(2)	0.91(2)
N(3)-C(12)	1.281(2)
N(3)-C(11)	1.475(2)
C(6)-C(7)	1.513(3)
C(6)-H(1)	0.9900
C(6)-H(23)	0.9900
C(7)-C(8)	1.510(3)
C(7)-H(22)	0.9900
C(7)-H(21)	0.9900
C(8)-H(19)	0.9900
C(8)-H(20)	0.9900
C(9)-C(10)	1.523(3)
C(9)-H(4)	0.9900
C(9)-H(18)	0.9900
C(10)-C(11)	1.513(3)
C(10)-H(17)	0.9900
C(10)-H(16)	0.9900
C(11)-H(14)	0.9900
C(11)-H(15)	0.9900
C(12)-C(13)	1.502(3)
C(12)-C(14)	1.526(3)
C(14)-C(16)	1.531(3)
C(14)-C(15)	1.534(3)
C(16)-H(5)	0.9800
C(16)-H(6)	0.9800
C(16)-H(7)	0.9800
C(15)-H(9)	0.9800
C(15)-H(8)	0.9800
C(15)-H(10)	0.9800
C(13)-H(13)	0.9800
C(13)-H(12)	0.9800
C(13)-H(11)	0.9800
C(4)-C(5)	1.511(3)
C(4)-C(1)	1.531(3)
C(1)-C(3)	1.533(3)
C(1)-C(2)	1.537(3)
C(2)-H(25)	0.9800

C(2)-H(24)	0.9800
C(2)-H(26)	0.9800
C(3)-H(28)	0.9800
C(3)-H(29)	0.9800
C(3)-H(27)	0.9800
C(5)-H(32)	0.9800
C(5)-H(31)	0.9800
C(5)-H(30)	0.9800

N(1)-Fe(1)-N(2)	83.80(6)
N(1)-Fe(1)-N(3)	172.81(6)
N(2)-Fe(1)-N(3)	90.96(6)
N(1)-Fe(1)-S(2)	81.21(4)
N(2)-Fe(1)-S(2)	107.79(4)
N(3)-Fe(1)-S(2)	105.16(4)
N(1)-Fe(1)-S(1)	97.68(5)
N(2)-Fe(1)-S(1)	125.70(4)
N(3)-Fe(1)-S(1)	81.36(4)
S(2)-Fe(1)-S(1)	126.17(2)
C(14)-S(1)-Fe(1)	97.97(6)
C(1)-S(2)-Fe(1)	97.89(6)
C(4)-N(1)-C(6)	123.88(17)
C(4)-N(1)-Fe(1)	121.50(13)
C(6)-N(1)-Fe(1)	114.61(12)
C(9)-N(2)-C(8)	110.64(14)
C(9)-N(2)-Fe(1)	115.33(11)
C(8)-N(2)-Fe(1)	117.10(12)
C(9)-N(2)-H(2)	104.6(13)
C(8)-N(2)-H(2)	105.2(13)
Fe(1)-N(2)-H(2)	102.2(14)
C(12)-N(3)-C(11)	118.62(15)
C(12)-N(3)-Fe(1)	119.23(12)
C(11)-N(3)-Fe(1)	122.11(11)
N(1)-C(6)-C(7)	110.51(16)
N(1)-C(6)-H(1)	109.5
C(7)-C(6)-H(1)	109.5
N(1)-C(6)-H(23)	109.5
C(7)-C(6)-H(23)	109.5
H(1)-C(6)-H(23)	108.1
C(8)-C(7)-C(6)	115.87(18)
C(8)-C(7)-H(22)	108.3
C(6)-C(7)-H(22)	108.3
C(8)-C(7)-H(21)	108.3
C(6)-C(7)-H(21)	108.3
H(22)-C(7)-H(21)	107.4
N(2)-C(8)-C(7)	113.82(16)
N(2)-C(8)-H(19)	108.8
C(7)-C(8)-H(19)	108.8
N(2)-C(8)-H(20)	108.8
C(7)-C(8)-H(20)	108.8
H(19)-C(8)-H(20)	107.7

N(2)-C(9)-C(10)	110.97(15)
N(2)-C(9)-H(4)	109.4
C(10)-C(9)-H(4)	109.4
N(2)-C(9)-H(18)	109.4
C(10)-C(9)-H(18)	109.4
H(4)-C(9)-H(18)	108.0
C(11)-C(10)-C(9)	113.99(15)
C(11)-C(10)-H(17)	108.8
C(9)-C(10)-H(17)	108.8
C(11)-C(10)-H(16)	108.8
C(9)-C(10)-H(16)	108.8
H(17)-C(10)-H(16)	107.7
N(3)-C(11)-C(10)	111.53(15)
N(3)-C(11)-H(14)	109.3
C(10)-C(11)-H(14)	109.3
N(3)-C(11)-H(15)	109.3
C(10)-C(11)-H(15)	109.3
H(14)-C(11)-H(15)	108.0
N(3)-C(12)-C(13)	123.15(17)
N(3)-C(12)-C(14)	119.91(16)
C(13)-C(12)-C(14)	116.93(16)
C(12)-C(14)-C(16)	107.90(15)
C(12)-C(14)-C(15)	111.45(15)
C(16)-C(14)-C(15)	108.57(16)
C(12)-C(14)-S(1)	111.33(13)
C(16)-C(14)-S(1)	109.03(13)
C(15)-C(14)-S(1)	108.51(13)
C(14)-C(16)-H(5)	109.5
C(14)-C(16)-H(6)	109.5
H(5)-C(16)-H(6)	109.5
C(14)-C(16)-H(7)	109.5
H(5)-C(16)-H(7)	109.5
H(6)-C(16)-H(7)	109.5
C(14)-C(15)-H(9)	109.5
C(14)-C(15)-H(8)	109.5
H(9)-C(15)-H(8)	109.5
C(14)-C(15)-H(10)	109.5
H(9)-C(15)-H(10)	109.5
H(8)-C(15)-H(10)	109.5
C(12)-C(13)-H(13)	109.5
C(12)-C(13)-H(12)	109.5
H(13)-C(13)-H(12)	109.5
C(12)-C(13)-H(11)	109.5
H(13)-C(13)-H(11)	109.5
H(12)-C(13)-H(11)	109.5
N(1)-C(4)-C(5)	123.72(18)
N(1)-C(4)-C(1)	117.98(16)
C(5)-C(4)-C(1)	118.19(17)
C(4)-C(1)-C(3)	113.11(17)
C(4)-C(1)-C(2)	106.97(15)
C(3)-C(1)-C(2)	109.49(16)

C(4)-C(1)-S(2)	110.41(13)
C(3)-C(1)-S(2)	108.10(13)
C(2)-C(1)-S(2)	108.69(13)
C(1)-C(2)-H(25)	109.5
C(1)-C(2)-H(24)	109.5
H(25)-C(2)-H(24)	109.5
C(1)-C(2)-H(26)	109.5
H(25)-C(2)-H(26)	109.5
H(24)-C(2)-H(26)	109.5
C(1)-C(3)-H(28)	109.5
C(1)-C(3)-H(29)	109.5
H(28)-C(3)-H(29)	109.5
C(1)-C(3)-H(27)	109.5
H(28)-C(3)-H(27)	109.5
H(29)-C(3)-H(27)	109.5
C(4)-C(5)-H(32)	109.5
C(4)-C(5)-H(31)	109.5
H(32)-C(5)-H(31)	109.5
C(4)-C(5)-H(30)	109.5
H(32)-C(5)-H(30)	109.5
H(31)-C(5)-H(30)	109.5

Table S5. Anisotropic displacement parameters (A^2 x 10^3) for [$Fe^{II}(S_2{}^{Me2}N_3(Pr,Pr)$] (**1**). The anisotropic displacement factor exponent takes the form:
-2 pi^2 [h^2 a*^2 U11 + ... + 2 h k a* b* U12]

	U11	U22	U33	U23	U13	U12
Fe(1)	13(1)	13(1)	11(1)	-1(1)	1(1)	-1(1)
S(1)	14(1)	23(1)	15(1)	-2(1)	2(1)	3(1)
S(2)	15(1)	21(1)	14(1)	-4(1)	2(1)	-5(1)
N(1)	17(1)	15(1)	17(1)	1(1)	5(1)	-2(1)
N(2)	14(1)	15(1)	16(1)	-1(1)	0(1)	-1(1)
N(3)	12(1)	15(1)	13(1)	-2(1)	1(1)	-1(1)
C(6)	24(1)	23(1)	23(1)	0(1)	9(1)	-7(1)
C(7)	28(1)	22(1)	25(1)	1(1)	7(1)	-9(1)
C(8)	20(1)	17(1)	24(1)	-2(1)	3(1)	-6(1)
C(9)	18(1)	15(1)	15(1)	-3(1)	0(1)	2(1)
C(10)	14(1)	18(1)	19(1)	-3(1)	3(1)	5(1)
C(11)	15(1)	19(1)	16(1)	-3(1)	4(1)	1(1)
C(12)	14(1)	16(1)	15(1)	-2(1)	0(1)	-5(1)
C(14)	16(1)	16(1)	16(1)	-1(1)	-2(1)	1(1)
C(16)	22(1)	19(1)	28(1)	-4(1)	-1(1)	0(1)
C(15)	20(1)	23(1)	22(1)	-1(1)	-4(1)	3(1)
C(13)	25(1)	23(1)	16(1)	3(1)	2(1)	2(1)
C(4)	22(1)	18(1)	15(1)	-1(1)	4(1)	2(1)
C(1)	19(1)	19(1)	14(1)	-5(1)	1(1)	-1(1)
C(2)	24(1)	19(1)	22(1)	-5(1)	3(1)	-1(1)
C(3)	25(1)	36(1)	20(1)	-9(1)	-3(1)	1(1)
C(5)	46(1)	40(1)	16(1)	-3(1)	8(1)	-12(1)

Table S6. Hydrogen coordinates (x 10^4) and isotropic displacement parameters (A^2 x 10^3)

	x	y	z	U(eq)
H(1)	36	3657	2260	28
H(23)	265	3421	2979	28
H(22)	1077	1679	2630	30
H(21)	305	1204	2505	30
H(19)	959	600	1637	24
H(20)	418	1802	1433	24
H(4)	1273	1918	530	19
H(18)	1832	981	899	19
H(17)	2475	3349	929	21
H(16)	2543	2311	331	21
H(14)	2357	4718	16	20
H(15)	1761	3690	-237	20
H(5)	1285	8177	960	34
H(6)	590	9006	799	34
H(7)	1150	8753	259	34
H(9)	143	7846	-321	32
H(8)	-375	7681	259	32
H(10)	-175	6306	-156	32
H(13)	1746	6024	-638	32
H(12)	1165	7234	-643	32
H(11)	971	5600	-796	32
H(25)	1085	7588	2382	33
H(24)	1763	8412	2602	33
H(26)	1229	7848	3118	33
H(28)	2208	6585	3641	40
H(29)	2731	7037	3095	40
H(27)	2629	5377	3269	40
H(32)	961	5651	3787	51
H(31)	1558	4474	3810	51
H(30)	795	4007	3627	51
H(2)	1753(11)	2400(20)	1721(10)	22(6)

Table S7. Pseudo First Order Kinetics Data for the Reaction Between Superoxo **4** and H-Atom Donors at -73 ˚C in THF.

Times (mins)	THF $\ln([Fe^{III}O_2]/[Fe^{III}O_2]_0)$	d_8 THF $\ln([Fe^{III}O_2]/[Fe^{III}O_2]_0)$	100 eq CHD Average $\ln([Fe^{III}O_2]/[Fe^{III}O_2]_0)$
0	-7.65009	-7.65009	-7.65009
1.25	-7.65942	-7.65081	-7.69376
2.5	-7.66879	-7.65377	-7.70334
3.75	-7.67332	-7.65612	-7.73313
5	-7.67827	-7.65774	-7.75703
6.25	-7.68162	-7.66211	-7.78065
7.5	-7.69603	-7.66543	-7.797011127
8.75	-7.70145	-7.66574	-7.815139034
10	-7.70745	-7.66813	-7.834580414
11.25	-7.71859	-7.67183	-7.851362013
12.5	-7.72497	-7.67447	-7.877551753
13.75	-7.73520	-7.67786	-7.892110649
15	-7.74467	-7.67939	-7.925167001
16.25	-7.75596	-7.68098	-7.938535592
17.5	-7.76904	-7.68336	-7.954041008
18.75	-7.77708	-7.67853	-7.980115839
20	-7.79056	-7.68598	-8.005351005
21.25	-7.80292	-7.68118	-8.022785408
22.5	-7.81316	-7.68775	-8.042537874
23.75	-7.82368	-7.69144	-8.057485998
25	-7.83468	-7.69177	-8.071431519
26.25	-7.84971	-7.70025	-8.089041384
27.5	-7.86434	-7.69821	-8.10616687
28.75	-7.87601	-7.69987	-8.119832354
30	-7.88793	-7.70233	-8.136390529
31.25	-7.90332	-7.7022	-8.148086488
32.5	-7.91398	-7.70696	-8.158771961

[a]Monitored at λ= 523 nm by electronic absorption spectroscopy.

References.

(1) Stoll, S.; Schweiger, A. "EasySpin, a Comprehensive Software Package for Spectral Simulation and Analysis in EPR,"*J. Magn. Res.* **2006**, *178*, 42-55.

(2) Live, D. H.; Chan, S. I. "Evan's method for superconductncting solinoids,"*Anal. Chem.* **1970**, *42*, 791.

(3) Evans, D. A. "Evan's method,"*J. Chem. Soc.* **1959**, 2005.

(4) Ellison, J. J.; Nienstedt, A.; Shoner, S. C.; Barnhart, D.; Cowen, J. A., Kovacs, J. A. "Reactivity of Five-Coordinate Models for the Thiolate-Ligated Fe Site of Nitrile Hydratase,"*J. Am. Chem. Soc.* **1998**, *120*, 5691-5700.

(5) Bruker. APEX2 (Version 2.1-4), S. V. A., SADABS (Version 2007/4). 2007.

(6) Altomare, A. "SIR 92 – a program for automatic solution of crystal structures by direct methods. ,"*J. Appl. Crystallogr.* **1994**, *27*, 435–435

(7) Altomare, A.; Burla, C.; Camalli, M.; Cascarano, L.; Giacovazzo, C.; Guagliardi, A.; Moliterni, A. G. G.; Polidori, G.; Spagna, R. "SIR97: A new tool for crystal structure determination and refinement.,"*J. Appl. Cryst.* **1999**, *32*, 115-119.

(8) Sheldrick, G. M. In *SHELXL-97: Program for the Refinement of Crystal Structures* University of Gottingen, Germany., 1997.
(9) Sheldrick, G. M. "Crystal structure refinement with SHELXL.,"*Acta Crystallogr. Sect. C Struct. Chem.* **2015**, *71*, 3–8.
(10) Mackay, S.; Edwards, C.; Henderson, A.; Gilmore, C.; Stewart, N.; Shankland, K.; Donald, A. *MaXus: A Computer Program for the Solution Refinement of Crystal Structures from Diffraction Data*. University of Glasgow, Scotland. **1997**.
(11) Neese, F. "The ORCA program system,"*Interdiscip. Rev. Comput. Mol. Sci.* **2012**, *2*, 73-78.
(12) Grimme, S.; Ehrlich, S.; Goerigk, L. *J. Comput. Chem* **2011**, *32*, 1456-1465.
(13) Barone, V.; Cossi, M. "Quantum Calculation of Molecular Energies and Energy Gradients in Solution by a Conductor Solvent Model,"*J. Phys. Chem.* **1998**, *102*, 1995 -2001.
(14) Adamo, C.; Barone, V. "Toward reliable density functional methods without adjustable parameters: The PBE0 model,"*J. Chem. Phys.* **1999**, *110*, 6158 – 6170.
(15) Neese, F.; Wennmohs, F.; Hansen, A.; Becker, U. "Efficient, approximate and parallel Hartree-Fock and hybrid DFT calculations. A 'chain-of-spheres' algorithm for the Hartree-Fock exchange,"*Chem. Phys.* **2009**, *356*, 98–109.
(16) Villar-Acevedo, G.; Lugo-Mas, P.; Blakely, M. N.; Rees, J. A.; Ganas, A. S.; Hanada, E. M.; Kaminsky, W.; Kovacs, J. A. "Metal-Assisted Oxo Atom Addition to an Fe(III)-Thiolate.,"*J. Am. Chem. Soc.* **2017**, *139*, 119-129.
(17) Shearer, J.; Scarrow, R. C.; Kovacs, J. A. "Synthetic models for the cysteinate–ligated Non–Heme Iron Enzyme Superoxide Reductase: Observation and Structural characterization by XAS of an FeIII–OOH Intermediate,"*J. Am. Chem. Soc.* **2002**, *124*, 11709-11717.
(18) Villar-Acevedo, G.; Nam, E.; Fitch, S.; Benedict, J.; Freudenthal, J.; Kaminsky, W.; Kovacs, J. A. "Influence of Thiolate Ligands on Reductive N–O Bond Activation. Oxidative Addition of NO to a Biomimetic SOR Analogue, and its Proton-Dependent Reduction of Nitrite.,"*J. Am. Chem. Soc.* **2011**, *133*, 1419-1427.
(19) Kumar, D.; Sastry, G. N.; Goldberg, D. P.; de Visser, S. P. "Mechanism of S-Oxygenation by a Cysteine Dioxygenase Model Complex,"*J. Phys. Chem. A.* **2012**, *116*, 582-591.
(20) Soda, T.; Kitagawa, Y.; Onishi, T.; Takano, Y.; Shigeta, Y.; Nagao, H.; Yoshioka, Y.; Yamaguchi, K. "Ab initio computations of effective exchange integrals for H–H, H–He–H and Mn2O2 complex: comparison of broken-symmetry approaches,"*Chem. Phys. Lett.* **2000**, *319*, 223 – 230.
(21) Hirata, S.; Head-Gordon, M. "Time-dependent Density Functional Theory within the Tamm–Dancoff Approximation,"*Chem. Phys. Lett.* **1999**, *314*, 291− 299.
(22) Neese, F.; Olbrich, G. "Efficient use of the resolution of the identity approximation in time-dependent density functional calculations with hybrid density functionals,"*Chem. Phys. Lett.* **2002**, *362*, 170−178.
(23) Pettersen, E. F.; Goddard, T. D.; Huang, C. C.; Couch, G. S.; Greenblatt, D. M.; Meng, E. C.; Ferrin, T. E. "UCSF Chimera- a visualization system for exploratory research and analysis,"*J. Comput. Chem.* **2004**, *25*, 1605–1612.
(24) Luo, Y.-R. *Comprehensive Handbook of Chemical Bond Energies*; Taylor and Francis Group: Boca Raton, FL, 2007.
(25) Paulsen, C. E.; Truong, T. H.; Garcia, F. J.; Homann, A.; Gupta, V.; Leonard, S.; Carroll, K. S. "Peroxide-dependent sulfenylation of the EGFR catalytic site enhances kinase activity,"*Nature Chem. Biol.* **2012**, *8*, 57-64.
(26) Leonard, S. E.; Reddie, K. G.; Carroll, K. S. "Mining the Thiol Proteome for Sulfenic Acid Modifications Reveals New Targets for Oxidation in Cells,"*ACS Chem. Biol.* **2009**, *4*, 783-799.